Paper No.
04623

CORROSION2004

MODELING OF CO_2 CORROSION OF MILD STEEL AT HIGH PRESSURES OF CO_2 AND IN THE PRESENCE OF ACETIC ACID

Keith George, Shihuai Wang , Srdjan Nesic and Kees de Waard
Institute for Corrosion and Multiphase Technology
Ohio University, Athens, OH 45701

ABSTRACT

Recently, experiments have been performed to determine the electrochemistry of mild steel at high pressures of carbon dioxide (CO_2) and in the presence of acetic acid (HAc). An electrochemical model which has been validated with data collected in glass cells will be compared to the new data which has been gathered in a high pressure flow loop Furthermore, the de Waard corrosion model has been modified to account for the presence of acetic acid and the predicted corrosion rated from the de Waard model will also be compared to the experimental corrosion rate data found by using linear polarization resistance (LPR) and weight loss measurements.

Key words: acetic acid, potentiodynamic sweeps, corrosion modeling, electrochemical modeling.

INTRODUCTION

Numerous corrosion prediction models have been developed throughout the years in an attempt at quantifying the risk of CO_2 corrosion.[1-8] These models are largely empirical or semi-empirical correlations from either field data, laboratory data or a combination of the two. A limitation to these models appears when additional data about existing or new phenomena become available (such as the effect of organic acids discussed below) and then cannot easily be incorporated into the models without recalibration of the entire model. This can be difficult and often a time consuming exercise with an uncertain outcome.

Another approach to CO_2 corrosion modeling is exemplified by the so called mechanistic models[9-10] which are developed on solid engineering/scientific grounds. Mechanistic models also include unknown constants, which must be estimated by comparison to experimental data, however these constants have clear physical meaning and usually do not need as frequent adjustments whenever new data emerge or new phenomena are incorporated into the model. The main "drawback" with mechanistic models is that they cannot be formulated successfully unless there is sufficient understanding about the phenomena

being modeled, a problem not encountered by the purely empirical models. As the name suggests, semi-empirical models are somewhere in between.

A limitation of all existing CO_2 corrosion models is that they are predominantly based on laboratory data, generated in glass cell or small diameter flow loop experiments. While a wide range of experimental parameters can be covered in such equipment (temperatures, pH, flow rates) most in depth electrochemical studies have been limited to glass cells and low partial pressures of CO_2. (typically ≤1 bar). Since limited experimental data exist at high CO_2 partial pressures, the models based on low pressure data have to extrapolate to these conditions. Their application to complex field conditions is an even more uncertain exercise.

Recently, new experimental data have been generated which offer an insight into the mild steel corrosion mechanisms and rates at high partial pressures of CO_2 and in the presence of HAc.[11] These data were generated with the primary intention of verifying and adjusting the existing mechanistic models for better corrosion rate prediction under these conditions. The experimental procedures and discussion of the results are described in the original publication[11] and will not be repeated here. The details of the electrochemical model and the modified de Waard (GDN) model has also been given elsewhere[12] and only the outline of the models will be shown below followed by the predictions and the discussion.

MODELS

Electrochemical model

In the model briefly described below it has been assumed that the main cathodic reaction is H^+ reduction and that H_2CO_3 and HAc act primarily as additional sources of H^+ ions (through dissociation). The only anodic reaction considered below is iron dissolution. Hence one can write the current density vs. voltage equation for H^+ reduction as:

$$\frac{1}{i_{(H^+)}} = \frac{1}{i_{a(H^+)}} + \frac{1}{i^d_{\lim(H^+)} + i^d_{\lim(HAc)} + i^r_{\lim(H_2CO_3)}} \quad (1)$$

where $i_{a(H+)}$ is the charge transfer current density in A/m^2, $i^d_{lim(H+)}$ is the mass transfer limiting current density for H^+ ions in A/m^2, $i^d_{\lim(HAc)}$ is the mass transfer limiting current density arising from the presence of HAc in A/m^2, and $i^r_{\lim(H_2CO_3)}$ is the chemical reaction limiting current density arising from the presence of H_2CO_3 in A/m^2.

The charge transfer current density in Equation (1) is given by the Tafel relationship:

$$i_{a(H^+)} = i_{0(H^+)} \times 10^{-\frac{\eta}{b_c}} \quad (2)$$

where $i_{0(H+)}$ is the exchange current density in A/m^2, η is the overvoltage in V, and b_c is the cathodic Tafel slope in V/dec.

The H^+ mass transfer limiting current density in Equation (1) is calculated by:

$$i^{d}_{\lim(H^+)} = k_m F[H^+]_b \tag{3}$$

where k_m is the H^+ mass transfer coefficient in m/s, F is Faraday's constant and $[H^+]_b$ is the bulk concentration of H^+ ions in kmol/m^3.

Similarly the HAc mass transfer limiting current density in Equation (1) is given by:

$$i^{d}_{\lim(HAc)} = k_m F[HAc]_b \tag{4}$$

where k_m is the HAc mass transfer coefficient in m/s, $[HAc]_b$ is the bulk concentration of HAc in kmol/m^3.

The H_2CO_3 chemical reaction current limiting current density in Equation (1) is found as:

$$i^{r}_{\lim(H_2CO_3)} = F[CO_2]_b \sqrt{D_{H_2CO_3} K_{hyd} k^{f}_{hyd}}\, f \tag{5}$$

where $[CO_2]_b$ is the bulk concentration of carbon dioxide in kmol/m^3, $D_{H_2CO_3}$ is the diffusion coefficient of H_2CO_3 in m^2/s, K_{hyd} is the equilibrium constant for carbon dioxide hydration s^{-1}, k^{f}_{hyd} is the rate of hydration of carbon dioxide in s^{-1} and f is the flow multiplier.

The only anodic reaction considered, iron dissolution, was assumed to be under activation control and hence pure Tafel behavior was modeled. The current density vs. voltage equation is then:

$$i_{(Fe)} = i_{0(Fe)} \times 10^{\frac{\eta}{b_a}} \tag{6}$$

where $i_{0(Fe)}$ is the exchange current density in A/m^2, η is the overvoltage in V, and b_a is the anodic Tafel slope in V/dec.

The corrosion potential then is found by solving the charge balance equation at the metal surface:

$$i_{(Fe)} = i_{(H^+)} \tag{7}$$

Direct reduction of water was neglected here. Once the corrosion potential is obtained from Equation (7), the corrosion current is found from the anodic current density (Equation 6) at the corrosion potential. More details about this model and its origins can be found elsewhere.[12]

George, de Waard, Nesic (GDN) model

The well-known de Waard model modified recently[12], for the presence of HAc, takes the following form:

$$\frac{1}{V_{corr}} = \frac{1}{V_r} + \frac{1}{V_{m_{(H2CO3)}} + V_{m_{(HAc)}}} \tag{8}$$

where V_{corr} is the corrosion rate in mm/yr, V_r is the reaction rate in mm/yr, $V_{m(H2CO3)}$ is the mass transfer rate of H_2CO_3 in mm/y, and $V_{m(HAc)}$ is the mass transfer rate of HAc in mm/yr.

The reaction rate in Equation (8) is:

$$\log(V_r) = c_1 + \frac{c_2}{T} + c_3 \log(pCO_2) + c_4 (pH_{actual} - pH_{CO_2}) \tag{9}$$

where pCO_2 is the partial pressure of CO_2 in bar, pH_{actual} is the actual system pH in the presence of cations such as Ca^{2+}, Fe^{2+}, Mg^{2+}, etc., pH_{CO2} is the "pure" pH of the system arising from CO_2 dissolution only and the c_1 to c_4 are constants.

The H_2CO_3 mass transfer component of the corrosion rate in Equation (8) can be found as:

$$V_{m_{(H2CO3)}} = c_5 \left(\frac{\nu^{0.8}}{d^{0.2}} \right) [pCO_2] \tag{10}$$

where ν is kinematic viscosity in m^2/s, d is pipe diameter in m and c_5 is a constant.

Finally the HAc mass transfer component of the corrosion rate in Equation (8)

$$V_{m(HAc)} = k_m [HAc] \tag{11}$$

More details about this model and its history can be found elsewhere.[12]

RESULTS AND DISCUSSION

Corrosion mechanisms

While both models described above can predict the corrosion rate, the electrochemical model offers additional insight into the corrosion mechanisms. Potentiodynamic sweeps predicted by the electrochemical model, shown in the figures below, have been "broken down" according to the three individual sources of hydrogen ions driving the cathodic reaction: (1) transport of hydrogen ions from the bulk, (2) transport and dissociation of carbonic acid and (3) transport and dissociation acetic acid. This was done in order to highlight the effect of the dominant corrosion mechanism. An example of a predicted potentiodynamic sweep is shown in Figure 1. It is clear that under these conditions HAc is the major source of hydrogen ions and is overshadowing the CO_2 corrosion process. In this and all other cases reported below, the role of pH, i.e. the "free" H^+ ions, is negligible. Also shown in Figure 1 is the sum of the cathodic currents (labeled: total cathodic). This figure will serve as a template for the comparison of the predicted and the experimental results given in subsequent figures. Unless otherwise specified all the results reported below were obtained for 60°C and at pH 5.

3 bar CO_2

The comparisons between the electrochemical model predictions and the experimental potentiodynamic sweeps at 3 bar CO_2 , without HAc, at velocities of 0.2 m/s, 1.0 m/s and 2.0 m/s are shown in Figures 2-4. At all three velocities, the potentiodynamic sweeps predicted by the electrochemical model were

found to be in good agreement with the experimental data. It is worth noting that in these figures only the H^+ reduction rate is significantly affected by the velocity. For example, at 0.2 m/s the limiting current is 0.08 A/m^2 but at 2.0 m/s, the limiting current shifts to 0.6 A/m^2 due to increased mass transfer of H^+ to the metal surface. The carbonic acid contribution to the limiting current is limited by CO_2 hydration kinetics and is not affected by the change in flow velocity. The anodic dissolution of iron is predicted well even if the experimental sweeps show evidence of prepassivation at higher overpotentials. This effect has not been modeled as it is suspected to be an artifact of the experimental technique used.

10 bar CO_2

For 10 bar CO_2, without HAc, the comparison between the electrochemical model and the experimental potentiodynamic sweeps at 0.2 and 2.0 m/s liquid velocities are shown in Figures 5 and 6. The electrochemical model and the experimental potentiodynamic sweeps are in remarkably good agreement given that this model was calibrated only with low pressure data making the predictions shown in Figure 5 and Figure 6 an extrapolation. It is worth noting that similar agreement was obtained at an intermediate liquid velocity of 1.0 m/s but is not shown here for brevity. At a partial pressure of 10 bar CO_2, the total limiting current shows no velocity dependence as it is dominated by a slow CO_2 hydration step.

20 bar CO_2

At 20 bar CO_2 and no HAc, the comparison between the electrochemical model and the experimental potentiodynamic sweeps at 0.2 and 2.0 m/s liquid velocity are shown in Figures 7 and 8. The electrochemical model predicts the corrosion behavior very well at all velocities studied (including 1 m/s experiment not shown). The discrepancy seen for the cathodic limiting current is probably due to an experimental artifact i.e. due to a rapid iron carbonate film formation on the working electrode during the cathodic sweeps.

10 ppm HAc

The comparison between the experimental data and the electrochemical model at 1 m/s, 10 bar CO_2 when 10 ppm HAc is present is shown in Figure 9. The corrosion process is dominated by H_2CO_3 i.e. by the high partial pressure of CO_2 while the 10 ppm of HAc make little difference in the corrosion mechanisms or rate. It is evident that the electrochemical model predicts the corrosion potential and cathodic limiting current very well. In all cases the electrochemical model predicts the charge-transfer region of the anodic region very well until prepassivation occurs at higher over-potentials.

100 ppm HAc

In the case of solutions containing 100 ppm HAc at 1m/s and 10 bar CO_2 (shown in Figure 10), the corrosion process seems to be still dominated by CO_2 (i.e. H_2CO_3) with HAc playing a larger role, contributing to approximately 15-20% of the total cathodic current. The model predicts the corrosion potential very well while the limiting current is slightly under-predicted when compared to the experimental data.

1000 ppm HAc

The comparison between the experimental data and the electrochemical model for solutions containing 1000 ppm HAc at 1 m/s and 10 bar CO_2 is shown in Figure 11. Again, the corrosion potential is predicted very well, but in this case, the experimental limiting current is not in good agreement with the electrochemical model. It is believed that the experimental potentiodynamic sweeps are faulty in these conditions due to the working electrode being rapidly filmed during the cathodic sweep. The corrosion process appears to be under mixed H_2CO_3-HAc control with HAc playing a somewhat more important role.

Under the same conditions and for liquid velocities of 0.2 and 2.0 m/s the comparisons are shown in Figures 12 and 13. As in the case of 1.0 m/s, the corrosion potentials are predicted very well but the limiting currents are not in agreement due to filming of the working electrode. It is worth remembering that the HAc limiting current is mass transfer controlled and is therefore sensitive to the liquid velocity while the one arising from H_2CO_3 is not. Therefore HAc which is a minor source of H^+ ions at 0.2 m/s actually becomes the main source of H^+ at 2.0 m/s.

Corrosion rates

Effects of velocity and CO_2 partial pressure

The comparison between the experimental data (LPR and weight loss) and the electrochemical and de Waard corrosion model at a partial pressure of 3 bar CO_2 is shown Figure 14. Since no HAc was present during the experiments, the data from experiments is compared to the de Waard corrosion model from 1995. The average value of the experimental data set is presented there, with the error bars representing the maximum and minimum experimental values. The number of independent experimental data points used to calculate the average is given above the error bar. It is evident that the experimental LPR and weight loss measurements are in good agreement with each other. It is also evident that only a slight velocity dependence can be seen in the experimentally corrosion rates. Both models predict the corrosion rate rather well particularly at the higher velocities. The de Waard corrosion model predicts too rapid a change in the corrosion rate with velocity and under-estimates the corrosion rate at 0.2 m/s. The electrochemical model shows the opposite trend, having virtually no velocity dependence and over-predicts the corrosion rates at 0.2 m/s.

The comparisons between the experimental data (LPR and weight loss) and the electrochemical and de Waard models at partial pressures of 10 and 20 bar CO_2 are shown in Figures 15 and 16. The de Waard model again shows a higher velocity dependence on the corrosion rate than experimentally observed while the electrochemical model again shows virtually no velocity dependence but is in good agreement with the experimental results.

Effects of HAc and velocity

The comparison between the experimental data (LPR and weight loss) and the electrochemical and GDN models as a function of HAc concentration are shown in Figure 17. Both models predict well the effect of HAc on the corrosion rate which becomes significant at 10 bar CO_2 only when HAc concentration exceeds 100 ppm. At all concentrations of HAc, both models slightly underpredict the experimental values, with the GDN model in slightly better agreement than the electrochemical model.

The effect of velocity on the corrosion rate of mild steel in the presence of 1000 ppm HAc is shown in Figure 18. Both models show the correct experimental trend i.e. the more significant velocity dependence of the corrosion rate when compared with the case of HAc-free CO_2 corrosion (shown in Figure 15). Interestingly, the strong velocity dependence is undepredicted by both models.

CONCLUSIONS

Weight loss and LPR measurements have been used to verify the basic effect of HAc on the anodic and cathodic reactions present in CO_2 corrosion found from potentiodynamic sweeps. The potentiodynamic sweeps were then compared with an electrochemical model. The agreement between the model and the experimental results is very good. A modification to the de Waard corrosion model has been made to account for the presence of HAc (GDN model). The experimental corrosion rates, measured using LPR and weight loss, were in agreement with the electrochemical and GDN models.

REFERENCES

1. C. de Waard, U. Lotz, "Prediction of CO_2 Corrosion in Carbon Steel", CORROSION/1993, Paper No. 69, (Houston, TX: NACE International 1993).
2. C. de Waard, U. Lotz, A. Dugstad, "Influence of Liquid Flow Velocity on CO_2 Corrosion: A Semi-Empirical Model", CORROSION/1995, Paper No. 128, (Houston, TX: NACE International, 1995).
3. Y.M. Gunaltun, "Combining Research and Field Data for Corrosion Rate Prediction", CORRODSION/1996, Paper No. 27, (Houston, TX: NACE International, 1996).
4. B.F.M. Pots, R.C. John, I.J. Rippon, M.J..S. Thomas, S.D. Kapusta, M.M. Girgis, T.Whitam, "Improvements on de Waard-Milliams Corrosion Prediction an Applications to Corrosion Management", CORROSION/2002, Paper No. 02235, (Houston, TX: NACE International, 2002).
5. E. Dayalan, G. Vani, J.R. Shadley, S.A. Shirazi, E.F. Ryicki, "CO_2 Corrosion of Carbon Steels in Pipe Flow", CORROSION/95, Paper No. 118, (Houston, TX: NACE International1995).
6. R.C. John, K.G. Jordan, A.L. Young, S.D. Kapusta, W.T. Thompson, "SweetCor: An Information System for the Analysis of Corosion of Steels by Water and Carbon Dioxide", CORROSION/98, Paper No. 20, (Houston, TX: NACE International, 1998).
7. W.P. Jepson, S. Stitzel, C. Kang, M. Gopal, "Model for Sweet Corrosion in Horizontal Multiphase Slug Flow", CORROSINO/97, Paper No. 11, (Houston, TX: NACE International, 1997).
8. B.F.M.Pots, "Mechanistic Models for the Prediction of CO_2 Corrosion Rates under Multiphase Flow Conditions", CORROSIN/95, Paper No. 137, (Houston, TX: NACE International, 1995).
9. S. Nesic, J. Postlethwaite, S. Olsen, "An Electrochemical Model for Prediction Of Corrosion of Mild Steel in Aqueous Carbon Dioxide Solutions," *Corrosion Science*, Vol 52, No 4, April 1996, p 280.
10. S. Nesic, M. Nordsveen, R. Nyborg, A. Stangeland, "A Mechanistic Model for CO_2 Corrosion with Protective Iron Carbonate Films", CORROSION/2001, Paper No. 01040, (Houston, TX: NACE International, 2001).
11. S. Wang, K. George, S. Nesic, "High Pressure CO_2 Electrochemistry and the Effect of Acetic Acid", CORROSION/2004, Paper No. 04375, (Houston, TX: NACE International, 2004).
12. K. George, S. Nesic, K. de Waard, "Electrochemical Invesitgation of CO_2 Corrosion of Mild Steel in the Presence of Acetic Acid", CORROSION/2004, Paper No. 04379, (Houston, TX: NACE International, 2004).

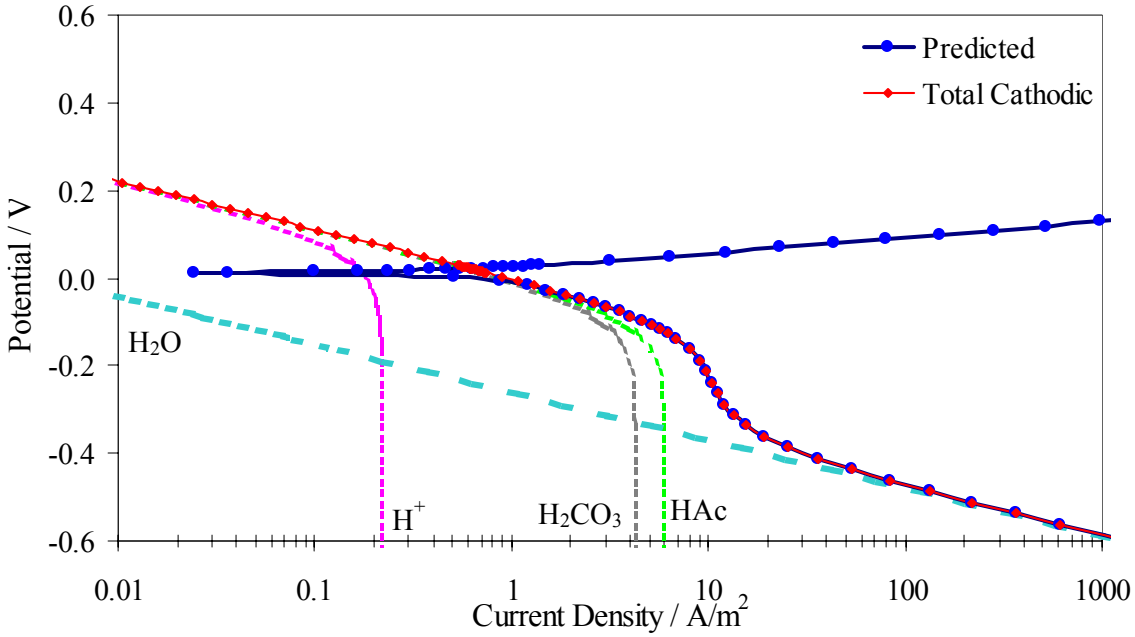

Figure 1. The predicted electrochemical reactions in pressurized solutions at a partial pressure of CO_2 of 3 bar containing 200 ppm HAc (60°C, pH 4.5, 1.0m/s).

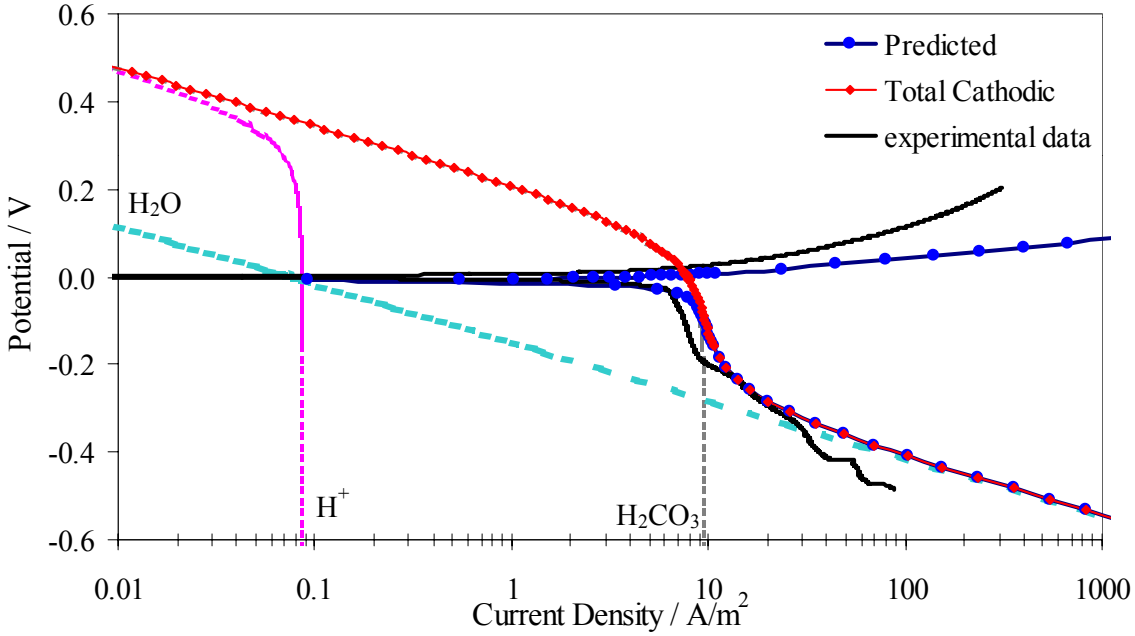

Figure 2. Comparison between the electrochemical model and experimental data at 3 bar CO_2 and a liquid velocity of 0.2 m/s (60°C, pH 5).

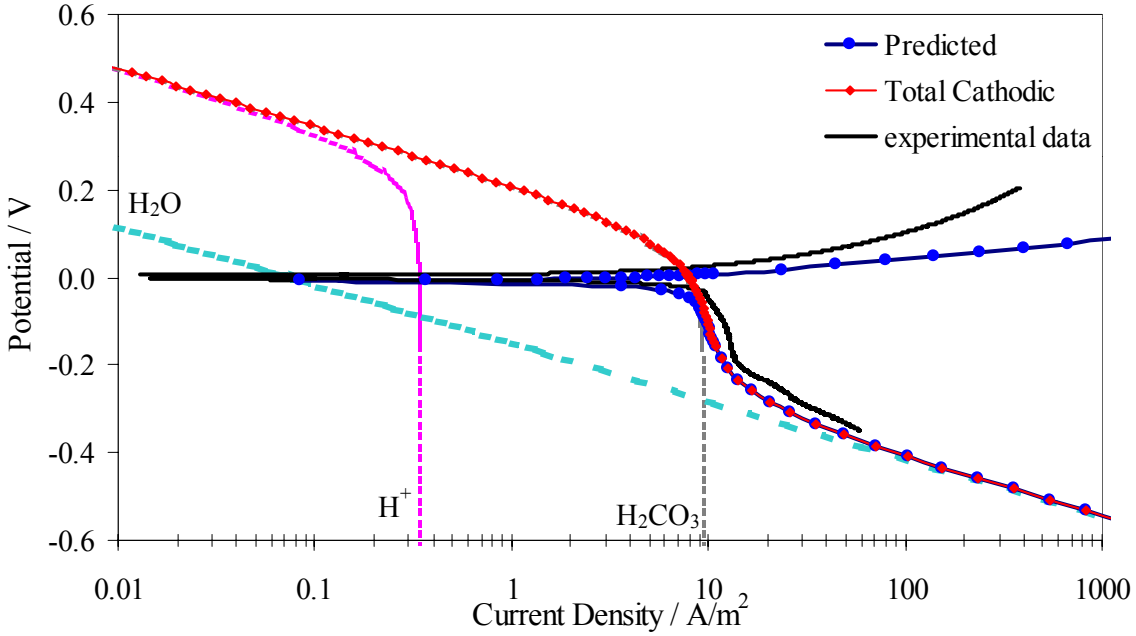

Figure 3. Comparison between the electrochemical model and experimental data at 3 bar CO_2 and a liquid velocity of 1.0 m/s (60°C, pH 5).

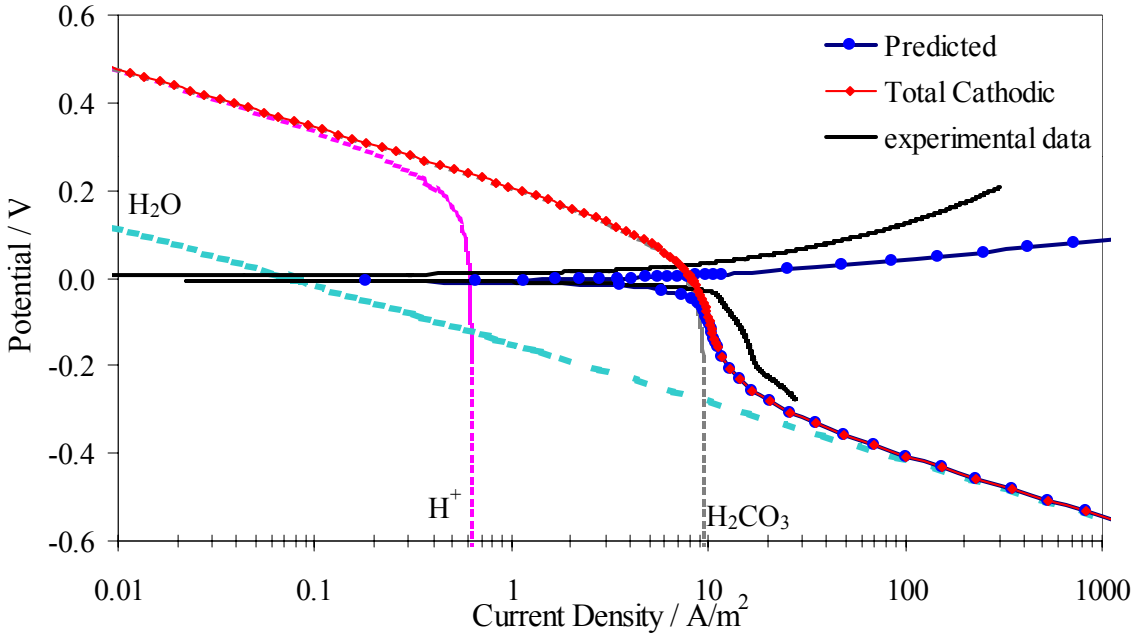

Figure 4. Comparison between the electrochemical model and experimental data at 3 bar CO_2 and a liquid velocity of 2.0 m/s (60°C, pH 5).

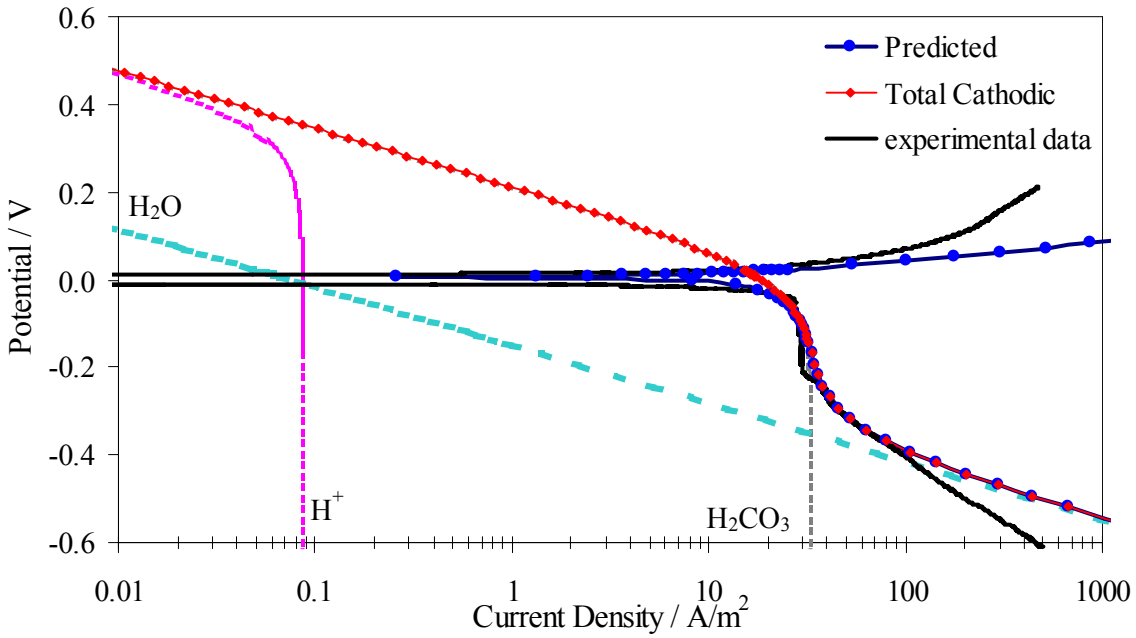

Figure 5. Comparison between the electrochemical model and experimental data at 10 bar CO_2 and a liquid velocity of 0.2 m/s (60°C, pH 5).

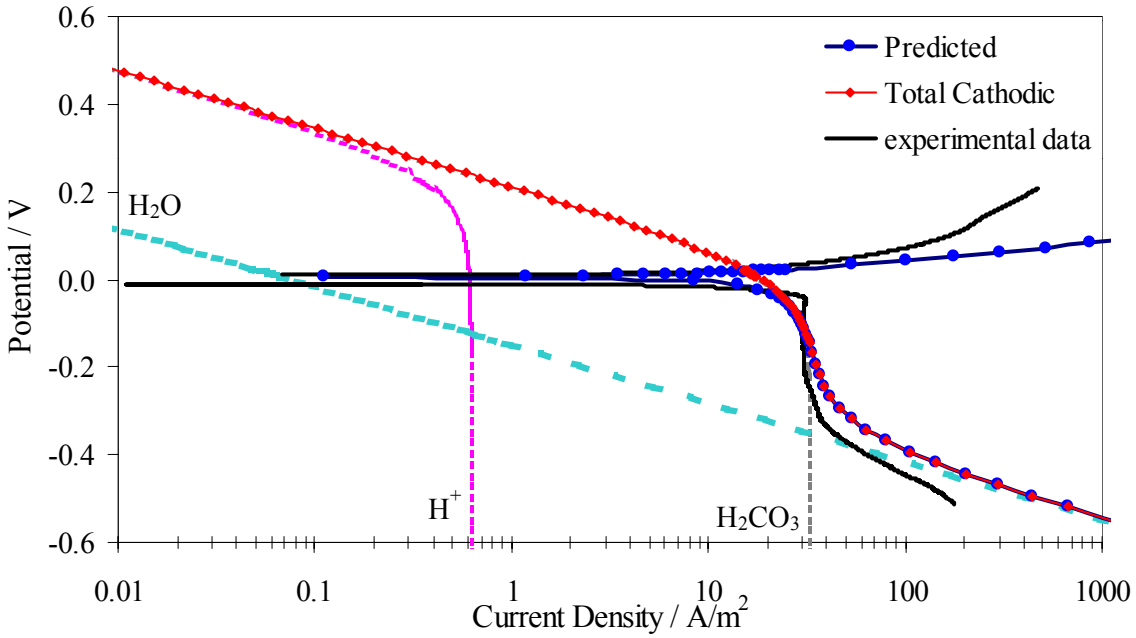

Figure 6. Comparison between the electrochemical model and experimental data at 10 bar CO_2 and a liquid velocity of 2.0 m/s (60°C, pH 5).

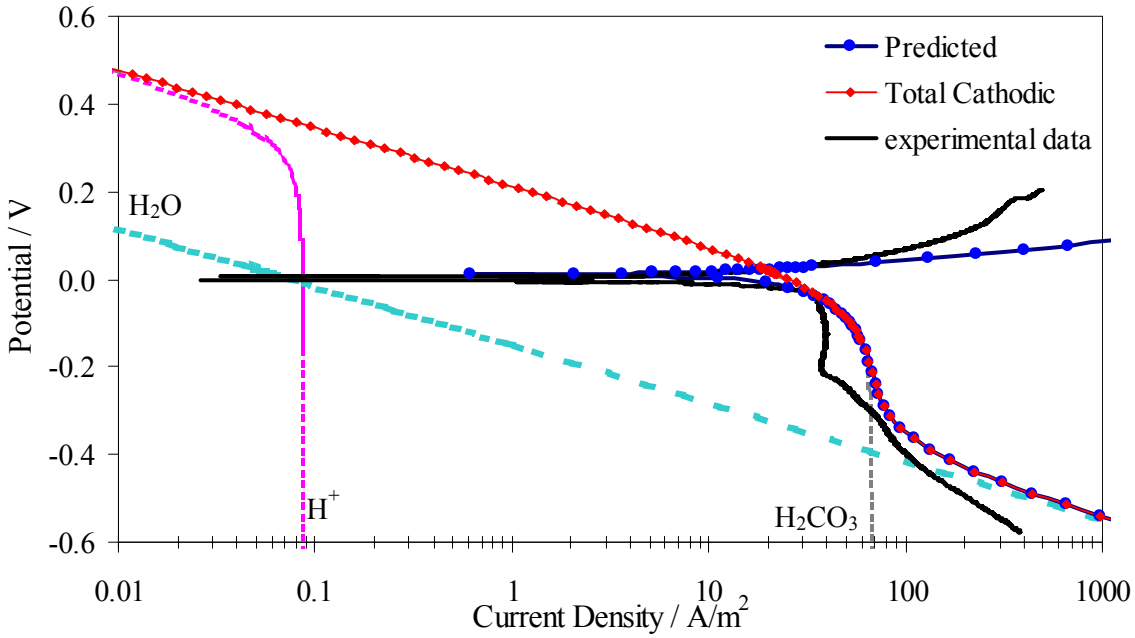

Figure 7. Comparison between the electrochemical model and experimental data at 20 bar CO_2 and a liquid velocity of 0.2 m/s (60°C, pH 5).

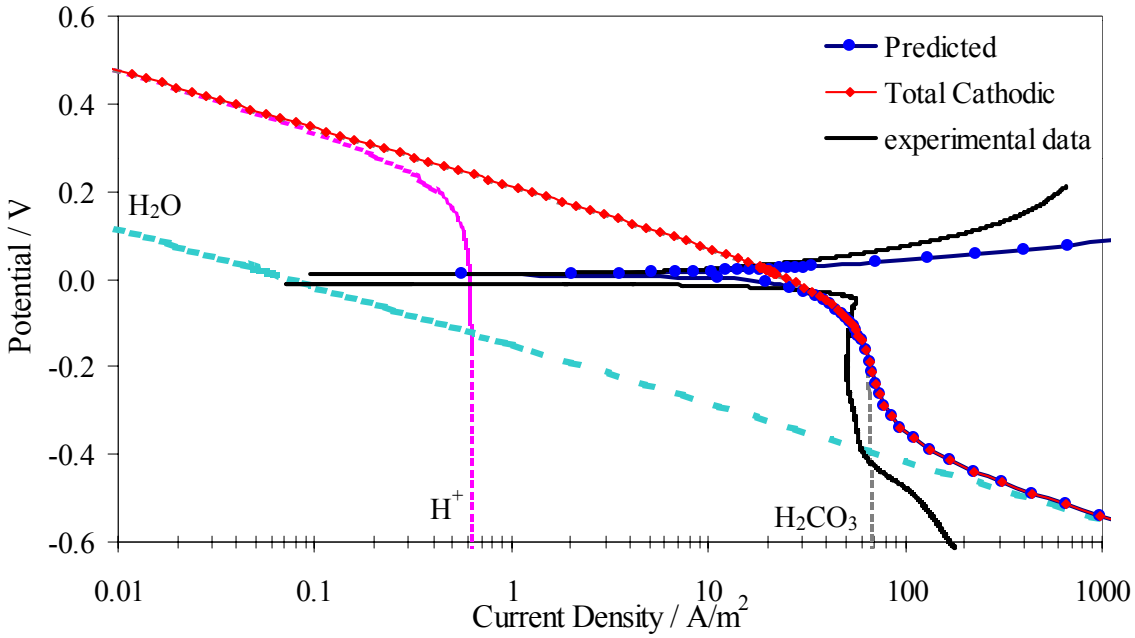

Figure 8. Comparison between the electrochemical model and experimental data at 20 bar CO_2 and a liquid velocity of 2.0 m/s (60°C, pH 5).

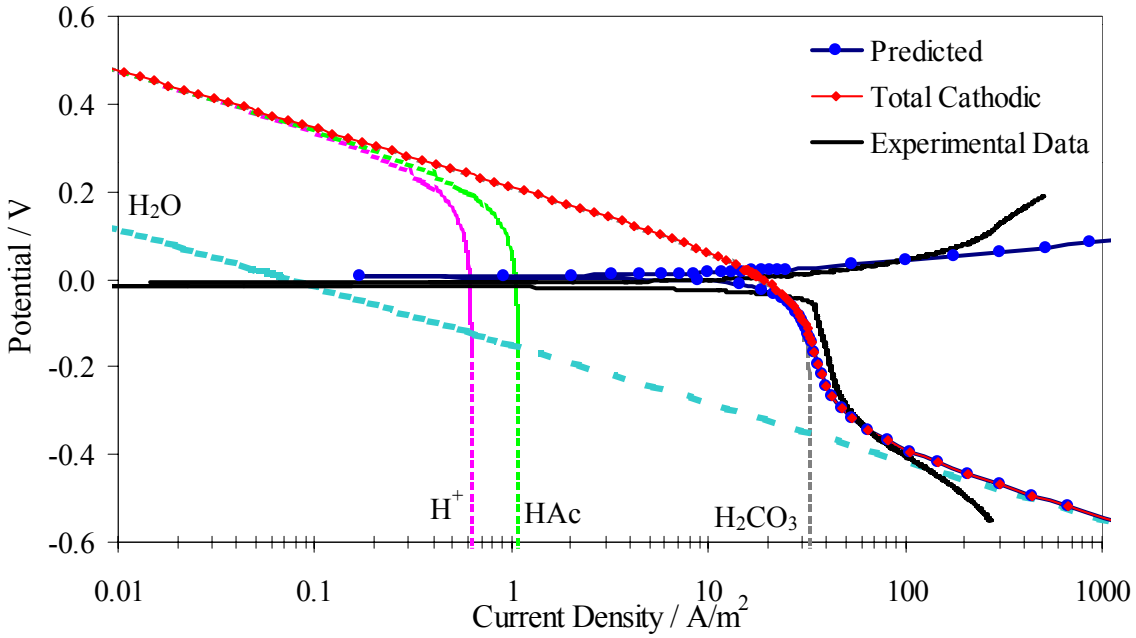

Figure 9. The comparison between the electrochemical model and the experimental data for 10 ppm HAc (60°C, pH 5, 1 m/s, 10 bar CO_2).

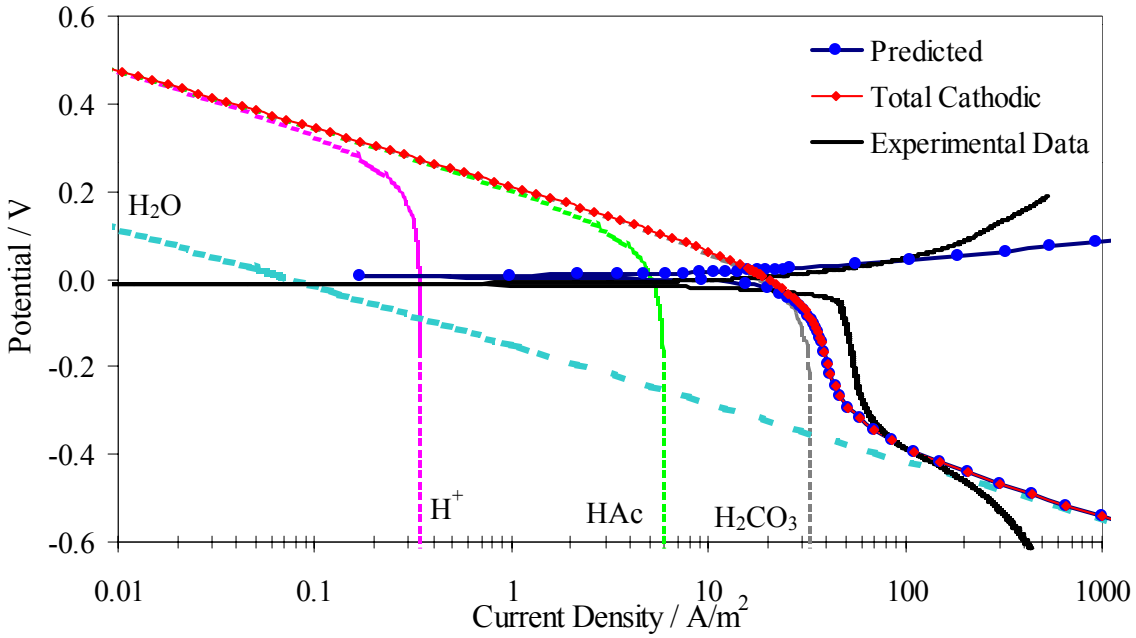

Figure 10. The comparison between the electrochemical model and the experimental data for 100 ppm HAc (60°C, pH 5, 1 m/s, 10 bar CO_2).

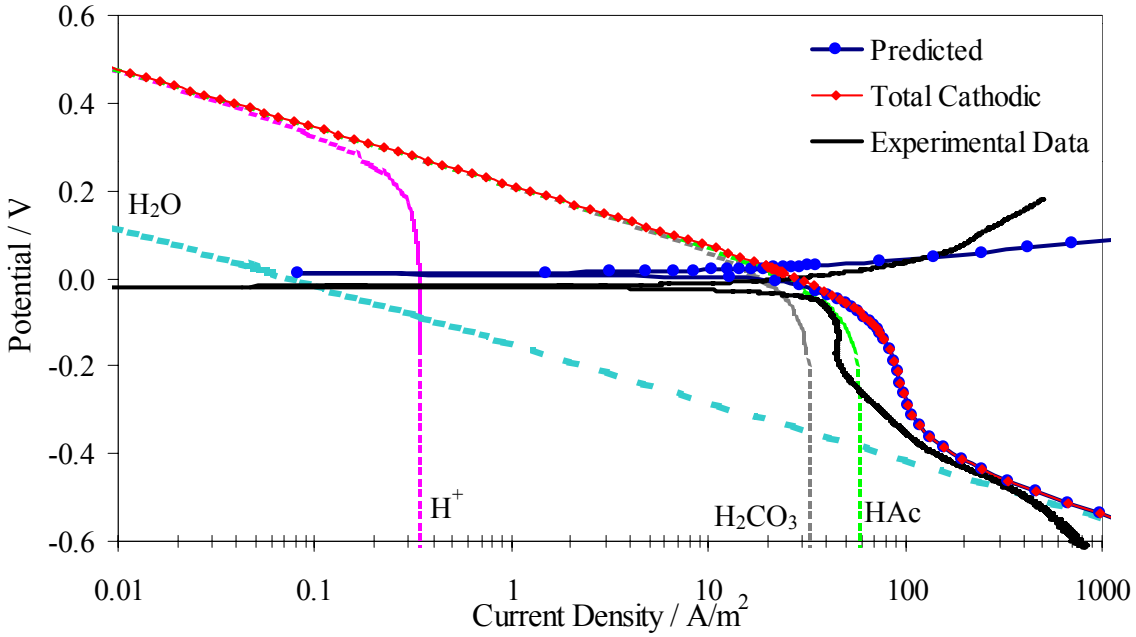

Figure 11. The comparison between the electrochemical model and the experimental data for 1000 ppm HAc (60°C, pH 5, 1 m/s, 10 bar CO_2).

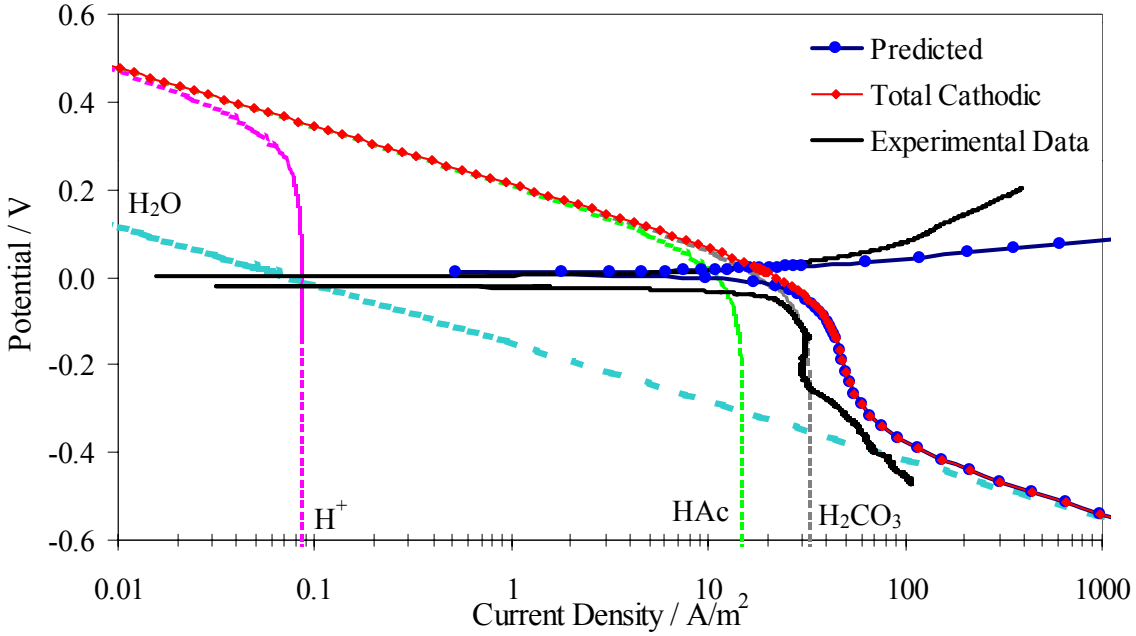

Figure 12. The comparison between the electrochemical model and the experimental data for 1000 ppm HAc at 0.2 m/s (60°C, pH 5, 10 bar CO_2).

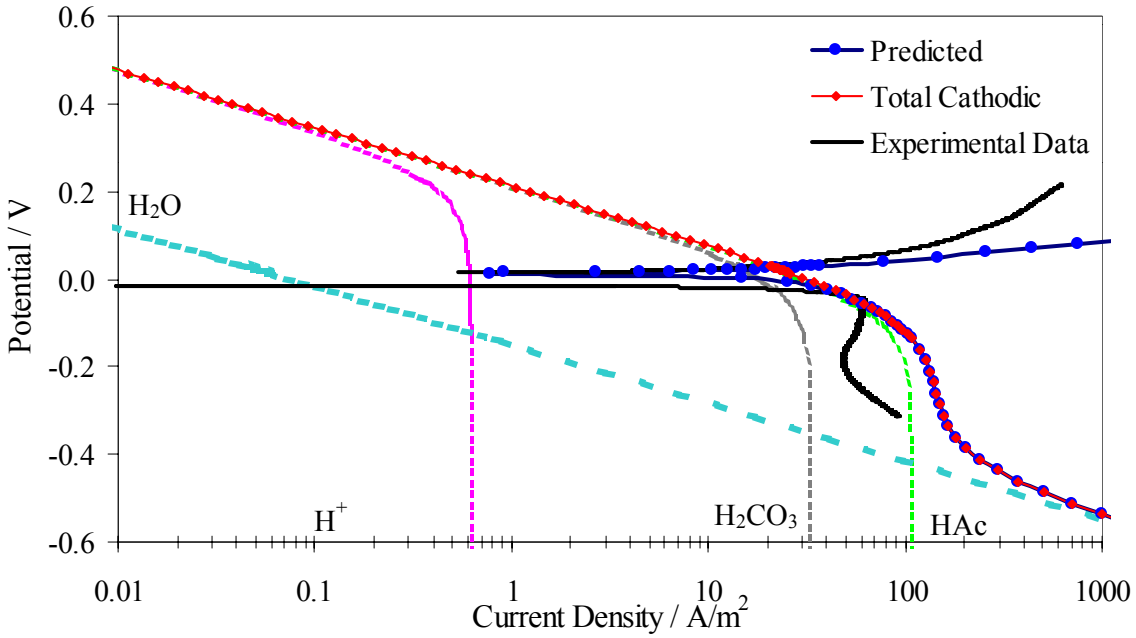

Figure 13. The comparison between the electrochemical model and the experimental data for 1000 ppm HAc at 2.0 m/s (60°C, pH 5, 10 bar CO_2).

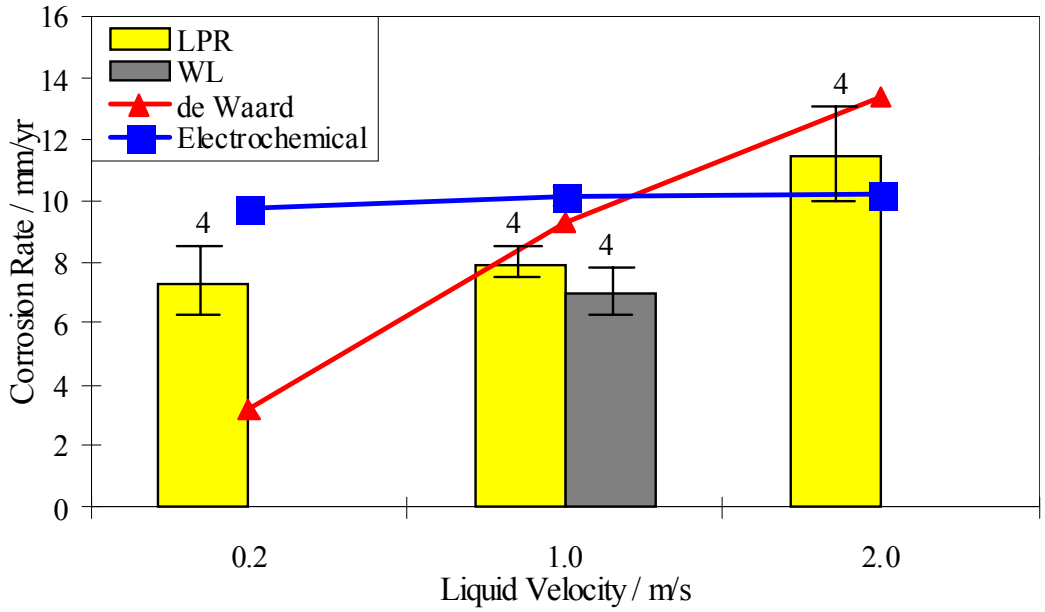

Figure 14. Comparison between the experimental LPR and weight loss data with the electrochemical and de Waard corrosion models at 3 bar CO_2 partial pressure (60°C, pH 5, 0.2-2.0 m/s). Error bars represent maximum and minimum experimental values.

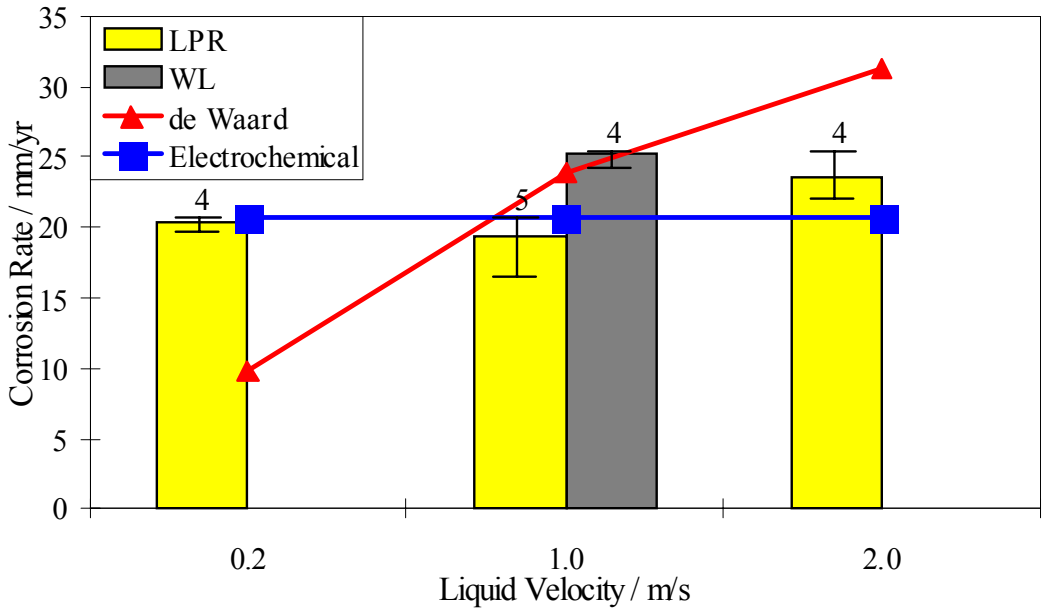

Figure 15. Comparison between the experimental LPR and weight loss data with the electrochemical and de Waard corrosion models at 10 bar CO_2 partial pressure (60°C, pH 5, 0.2-2.0 m/s). Error bars represent maximum and minimum experimental values.

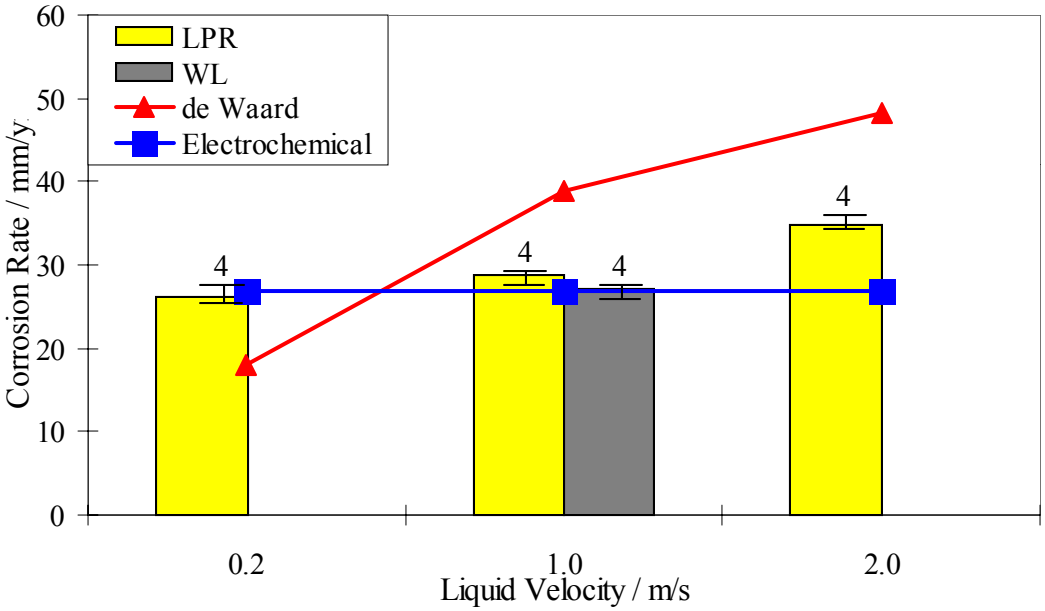

Figure 16. Comparison between the experimental LPR and weight loss data with the electrochemical and de Waard corrosion models at 20 bar CO_2 partial pressure (60°C, pH 5, 0.2-2.0 m/s). Error bars represent maximum and minimum experimental values.

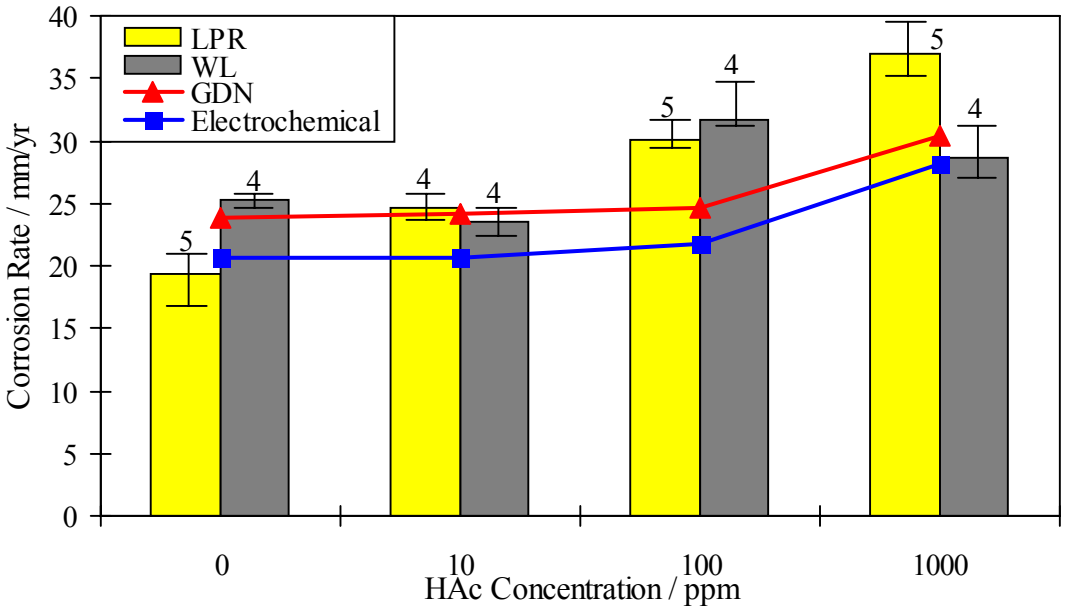

Figure 17. The comparison between the experimental LPR and weight loss data with the GDN and electrochemical models (0-1000 ppm, 60°C, pH 5, 1 m/s, 10 bar CO_2).

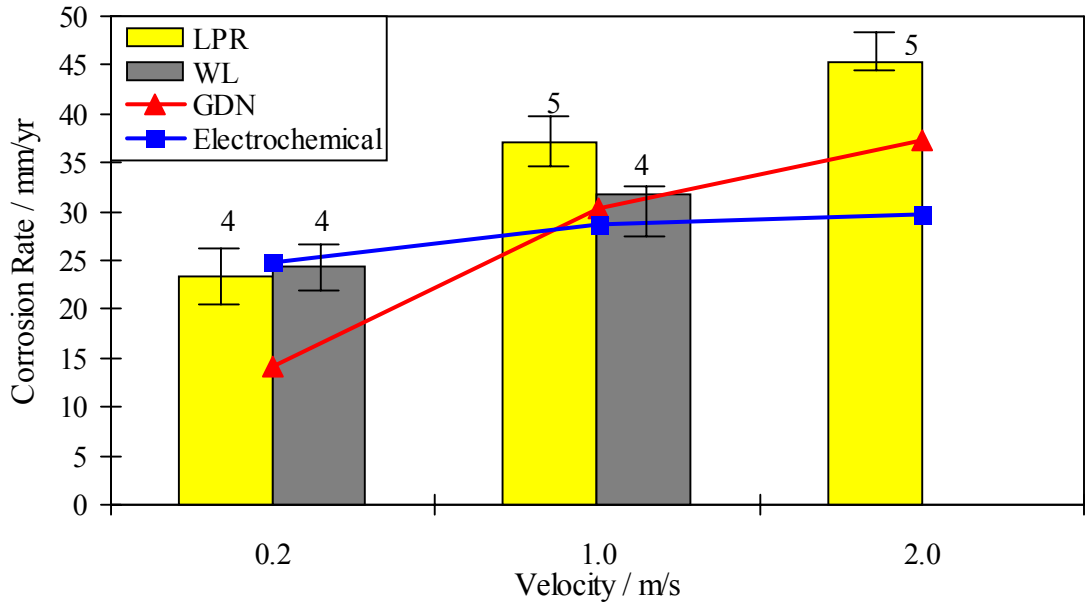

Figure 18. The comparison between the experimental LPR and weight loss data with the GDN and electrochemical model (1000 ppm HAc, 60°C, pH 5, 0.2-2.0 m/s, 10 bar CO_2).